Cytoplasmic localization of p35 and p39 may be closely correlated to formation and/or membrane trafficking of recycling endosomes and Golgi apparatus.

We demonstrated the regulation of intracellular localization of Cdk5-activator complexes through its activity. Most of the experiments were done by separate expression of p35 or p39 into COS-7 cells. Although there was a possibility that p35–Cdk5 and p39–Cdk5 regulate the respective localization of each other, the distribution of p39 was not affected by coexpression of p35 in cultured neurons, indicating that the results obtained with COS-7 cells can be applied to neurons. It is shown that Cdk5 plays a versatile function in neurons from the developmental stage to neurodegeneration. In developing neurons, p35–Cdk5 regulates neuronal activities in different cytoplasmic regions, nuclear migration around the centrosomal region, and growth cone movement at the top of neurites (Sasaki et al., 2002; Xie et al., 2003). p35–Cdk5 controls exocytosis/endocytosis at the presynaptic site and post-synaptic signaling in the postsynaptic density (Tomizawa et al., 2002; Wei et al., 2005). On the other hand, the phosphorylated state of Ser8 changes with aging (Hosokawa et al., 2010). Thus, subcellular localization of p35–Cdk5 and p39–Cdk5 should be regulated spatiotemporally depending on the functional states of neurons. Therefore, we believe a series of our studies on the subcellular localization is important for a complete understanding of Cdk5 functions.

Materials and Methods

Antibodies and chemicals

The anti-p35 antibody C64B10 was obtained from Cell Signaling Technology (Danvers, MA). The anti-p35 antibody C19 and anti-Cdk5 antibody C-8 was obtained from Santa Cruz Biotechnology (Santa Cruz, CA). The anti-myc antibody (4A6) was obtained from Millipore (Billerica, MA). The anti-β-tubulin antibody (TUB2.1) was purchased from Sigma (St Louis, MO). Secondary antibodies conjugated with Alexa Fluor 488 or Alexa Fluor 546 were purchased from Invitrogen (Carlsbad, CA). Horseradish peroxidase (HRP)-conjugated goat anti-mouse IgG and HRP-conjugated swine anti-rabbit IgG were purchased from Dako (Glostrup, Denmark). 4′,6-diamidino-2-phenylindole (DAPI) was purchased from Dojindo (Kumamoto, Japan). Phos-tag acrylamide and roscovitine were obtained from Wako Pure Chemical Industries (Osaka, Japan).

Construction of mammalian cell expression vectors

Mouse p35, p39 and their G2A mutant tagged with myc at the C-terminus were used throughout this study. Mouse Cdk5 tagged with HA at the N-terminus (Cdk5) and K33T mutant of Cdk5 (knCdk5) were reported previously (Asada et al., 2008). pCAGGS-p39 tagged with myc was constructed by inserting PCR-amplified p39 into a pCAGGS vector. The Ala or Glu mutants of p35 at Ser8 and/or Thr138 and those of p39 at Ser8, Thr84, Ser173, Ser205, Thr232 and/or Ser305 were constructed using the Quikchange site-directed mutagenesis kit (Stratagene, La Jolla, CA) using pcDNA3-mouse p35 or pcDNA3-mouse p39 tagged with myc as a template. The Ala mutant at Lys75–Lys78, consecutive Lys residues from amino acids 75–78 of p39, was constructed by PCR with 5′-GCTGCAGCAGCTGGCAGCAAAAAGG-TGACGCCC-3′ and 5′-GGCCGAGGCTGCCACTAGGCG-3′ as forward and reverse primers using pcDNA3–mouse p39 as a template. All PCR constructs were verified by DNA sequencing.

Mammalian cell culture and transfection

COS-7 cells and HEK293 cells were maintained as described previously (Asada et al., 2008). For immunoblotting, COS-7 cells or HEK293 cells were transfected with the indicated plasmids using PolyFect Transfection Reagent (Qiagen, Valencia, CA) according to the manufacturer's protocol. For visualization of immunofluorescence, COS-7 cells were transfected with the indicated plasmids using Lipofectamine 2000 (Invitrogen, Carlsbad, CA) according to the manufacturer's protocol.

Neuronal cultures and transfection

Cortical neurons were prepared from mouse brains at embryonic day 17 as described previously (Endo et al., 2009). The p35 knockdown vector was reported previously (Endo et al., 2009). The control scramble sequence used was 5′-CCACTCGACCAGATAAGACGC-3′. For immunoblotting, plasmids encoding p39-myc and p35 knockdown shRNA or control scramble shRNA sequences were transfected into cultured neuron using an Amaxa Nucleofector according to manufacturer protocol (Lonza, Cologne, Germany). For immunostaining, above plasmids were transfected into cultured neurons by a calcium phosphate method as described previously (Saito et al., 2007).

Immunofluorescence observation

COS-7 cells cultured on glass cover slips were fixed with 4% paraformaldehyde in phosphate-buffered saline (PBS) for 30 min at room temperature and incubated with anti-myc (1:500) for p35 and p39 or anti-Cdk5 (1:100) in PBS containing 5% normal goat serum and 0.1% Triton X-100 for 1 h followed by incubation with secondary antibodies coupled to Alexa Fluor 488 or Alexa Fluor 546 (1:500). Nuclei were stained with DAPI. Anti-p35 C64B10 antibody (1:200) was used for staining of endogenous p35 in cultured neurons. Cells were examined under a confocal laser-scanning LSM510 microscope (Carl Zeiss, Jena, Germany). To determine the nuclear or cytoplasmic location of p35 or p39, the fluorescence intensity in the nucleus and the cytoplasm was quantified using Zen (Zeiss) software. For statistical analysis, more than 300 cells were measured for each construct. To determine the perinuclear or whole cytoplasmic localization of p35 or p39, the fluorescence intensity in the perinuclear (F_p) and the middle region or peripheral cytoplasm (F_c) was quantified, and the ratio of F_p/F_c over 2.0 was defined as the perinuclear localization. For statistical analysis, more than 300 cells were measured for each construct.

Cell death was assessed by LDH activity in cultured medium, condensed nuclei after DAPI staining or terminal deoxytransferase-mediated dUTP nick end-labeling (TUNEL) staining of the nucleus using the In Situ Cell Death Detection Kit, POD (Roche Diagnostics, Tokyo, Japan) according to the manufacturer's protocol (Saito et al., 2007).

Cell fractionation, SDS–PAGE, Phos-tag SDS-PAGE and immunoblotting

COS-7 cells were disrupted in 20 mM MOPS, pH 7.2, 1 mM $MgCl_2$, 50 mM NaCl, 0.1 mM EGTA, 1 mM EDTA, 1 mM dithiothreitol, 10 μg/ml leupeptin, 0.2 mM Pefabloc SC by passing through a 27-gauge syringe needle. After brief centrifugation at 100 ***g*** for 5 min, the supernatants were centrifuged again at 100,000 ***g*** for 60 min at 4°C. Laemmli's SDS–PAGE was carried out with 12.5% polyacrylamide gels. Proteins were transferred to PVDF (Millipore) membranes using a semi-dry blotting apparatus. Phos-tag SDS-PAGE was performed with 7.5% polyacrylamide gels containing 50 μM or 150 μM Phos-tag and 100 μM $MnCl_2$ (Kinoshita et al., 2006). Proteins were transferred to PVDF membranes using a submarine blotting apparatus. Membranes were probed with the primary antibodies, anti-myc for myc-tagged p35 and p39, or anti-tubulin (1:5000) followed by a secondary antibody conjugated with horseradish peroxidase (HRP) (Asada et al., 2008). The reactions were detected using a Millipore Immobilon western chemiluminescent HRP substrate (Millipore) or an ECL system (GE Healthcare).

Acknowledgements

We thank Mitsunori Fukuda at Tohoku University, Japan for GFP-tagged Rab vectors, Rachel Thomas for editing the manuscript, and Toru Isse and Mamiko Mitsuhashi for preliminary experiments.

Funding

This work was supported in part by grants-in-aid for Scientific Research from the Ministry of Education, Culture, Sports, and Science and Technology of Japan [grant number 19057007 to S.H.].

Supplementary material available online at
http://jcs.biologists.org/lookup/suppl/doi:10.1242/jcs.100503/-/DC1

References

Asada, A., Yamamoto, N., Gohda, M., Saito, T., Hayashi, N. and Hisanaga, S. (2008). Myristoylation of p39 and p35 is a determinant of cytoplasmic or nuclear localization of active cyclin-dependent kinase 5 complexes. *J. Neurochem.* **106**, 1325-1336.

Chae, T., Kwon, Y. T., Bronson, R., Dikkes, P., Li, E. and Tsai, L. H. (1997). Mice lacking p35, a neuronal specific activator of Cdk5, display cortical lamination defects, seizures, and adult lethality. *Neuron* **18**, 29-42.

Chang, K. H., Multani, P. S., Sun, K. H., Vincent, F., de Pablo, Y., Ghosh, S., Gupta, R., Lee, H. P., Lee, H. G., Smith, M. A. et al. (2011). Nuclear envelope dispersion triggered by deregulated Cdk5 precedes neuronal death. *Mol. Biol. Cell* **22**, 1452-1462.

Cheung, Z. H., Fu, A. K. and Ip, N. Y. (2006). Synaptic roles of Cdk5: implications in higher cognitive functions and neurodegenerative diseases. *Neuron* **50**, 13-18.

Dhavan, R. and Tsai, L. H. (2001). A decade of CDK5. *Nat. Rev. Mol. Cell Biol.* **2**, 749-759.

Dingwall, C. and Laskey, R. A. (1991). Nuclear targeting sequences–a consensus? *Trends Biochem. Sci.* **16**, 478-481.

Endo, R., Saito, T., Asada, A., Kawahara, H., Ohshima, T. and Hisanaga, S. (2009). Commitment of 1-methyl-4-phenylpyrinidinium ion-induced neuronal cell death by proteasome-mediated degradation of p35 cyclin-dependent kinase 5 activator. *J. Biol. Chem.* **284**, 26029-26039.

Fu, A. K., Fu, W. Y., Ng, A. K., Chien, W. W., Ng, Y. P., Wang, J. H. and Ip, N. Y. (2004). Cyclin-dependent kinase 5 phosphorylates signal transducer and activator of transcription 3 and regulates its transcriptional activity. *Proc. Natl. Acad. Sci. USA* **101**, 6728-6733.

Fu, X., Choi, Y.-K., Qu, D., Yu, Y., Cheung, N. S. and Qi, R. Z. (2006). Identification of nuclear import mechanisms for the neuronal Cdk5 activator. *J. Biol. Chem.* **281**, 39014-39021.

Gong, X., Tang, X., Wiedmann, M., Wang, X., Peng, J., Zheng, D., Blair, L. A., Marshall, J. and Mao, Z. (2003). Cdk5-mediated inhibition of the protective effects of transcription factor MEF2 in neurotoxicity-induced apoptosis. *Neuron* **38**, 33-46.

Hallows, J. L., Chen, K., DePinho, R. A. and Vincent, I. (2003). Decreased cyclin-dependent kinase 5 (cdk5) activity is accompanied by redistribution of cdk5 and cytoskeletal proteins and increased cytoskeletal protein phosphorylation in p35 null mice. *J. Neurosci.* **23**, 10633-10644.

Hayashi, N. and Titani, K. (2010). N-myristoylated proteins, key components in intracellular signal transduction systems enabling rapid and flexible cell responses. *Proc. Jpn. Acad., Ser. B, Phys. Biol. Sci.* **86**, 494-508.

Herrup, K. and Yang, Y. (2007). Cell cycle regulation in the postmitotic neuron: oxymoron or new biology? *Nat. Rev. Neurosci.* **8**, 368-378.

Hisanaga, S. and Endo, R. (2010). Regulation and role of cyclin-dependent kinase activity in neuronal survival and death. *J. Neurochem.* **115**, 1309-1321.

Hisanaga, S., Uchiyama, M., Hosoi, T., Yamada, K., Honma, N., Ishiguro, K., Uchida, T., Dahl, D., Ohsumi, K. and Kishimoto, T. (1995). Porcine brain neurofilament-H tail domain kinase: its identification as cdk5/p26 complex and comparison with cdc2/cyclin B kinase. *Cell Motil. Cytoskeleton* **31**, 283-297.

Hosokawa, T., Saito, T., Asada, A., Fukunaga, K. and Hisanaga, S. (2010). Quantitative measurement of in vivo phosphorylation states of Cdk5 activator p35 by Phos-tag SDS-PAGE. *Mol. Cell. Proteomics* **9**, 1133-1143.

Humbert, S., Dhavan, R. and Tsai, L. H. (2000). p39 activates cdk5 in neurons, and is associated with the actin cytoskeleton. *J. Cell Sci.* **113**, 975-983.

Kamei, H., Saito, T., Ozawa, M., Fujita, Y., Asada, A., Bibb, J. A., Saido, T.-C., Sorimachi, H. and Hisanaga, S. (2007). Suppression of calpain-dependent cleavage of the CDK5 activator p35 to p25 by site-specific phosphorylation. *J. Biol. Chem.* **282**, 1687-1694.

Kim, D., Frank, C. L., Dobbin, M. M., Tsunemoto, R. K., Tu, W., Peng, P. L., Guan, J. S., Lee, B. H., Moy, L. Y., Giusti, P. et al. (2008). Deregulation of HDAC1 by p25/Cdk5 in neurotoxicity. *Neuron* **60**, 803-817.

Kinoshita, E., Kinoshita-Kikuta, E., Takiyama, K. and Koike, T. (2006). Phosphate-binding tag, a new tool to visualize phosphorylated proteins. *Mol. Cell. Proteomics* **5**, 749-757.

Ko, J., Humbert, S., Bronson, R. T., Takahashi, S., Kulkarni, A. B., Li, E. and Tsai, L. H. (2001). p35 and p39 are essential for cyclin-dependent kinase 5 function during neurodevelopment. *J. Neurosci.* **21**, 6758-6771.

Li, Z., David, G., Hung, K. W., DePinho, R. A., Fu, A. K. and Ip, N. Y. (2004). Cdk5/p35 phosphorylates mSds3 and regulates mSds3-mediated repression of transcription. *J. Biol. Chem.* **279**, 54438-54444.

Mahalakshmi, R. N., Nagashima, K., Ng, M. Y., Inagaki, N., Hunziker, W. and Béguin, P. (2007). Nuclear transport of Kir/Gem requires specific signals and importin alpha5 and is regulated by calmodulin and predicted serine phosphorylations. *Traffic* **8**, 1150-1163.

Maures, T. J., Su, H. W., Argetsinger, L. S., Grinstein, S. and Carter-Su, C. (2011). Phosphorylation controls a dual-function polybasic nuclear localization sequence in the adapter protein SH2B1β to regulate its cellular function and distribution. *J. Cell Sci.* **124**, 1542-1552.

McLaughlin, S. and Aderem, A. (1995). The myristoyl-electrostatic switch: a modulator of reversible protein-membrane interactions. *Trends Biochem. Sci.* **20**, 272-276.

Nikolic, M., Dudek, H., Kwon, Y. T., Ramos, Y. F. M. and Tsai, L. H. (1996). The cdk5/p35 kinase is essential for neurite outgrowth during neuronal differentiation. *Genes Dev.* **10**, 816-825.

Ohshima, T., Ward, J. M., Huh, C. G., Longenecker, G., Veeranna, Pant, H. C, Brady, R. O., Martin, L. J. and Kulkarni, A. B. (1996). Targeted disruption of the cyclin-dependent kinase 5 gene results in abnormal corticogenesis, neuronal pathology and perinatal death. *Proc. Natl. Acad. Sci. USA* **93**, 11173-11178.

Paglini, G., Pigino, G., Kunda, P., Morfini, G., Maccioni, R., Quiroga, S., Ferreira, A. and Cáceres, A. (1998). Evidence for the participation of the neuron-specific CDK5 activator P35 during laminin-enhanced axonal growth. *J. Neurosci.* **18**, 9858-9869.

Paglini, G., Peris, L., Diez-Guerra, J., Quiroga, S. and Cáceres, A. (2001). The Cdk5-p35 kinase associates with the Golgi apparatus and regulates membrane traffic. *EMBO Rep.* **2**, 1139-1144.

Patrick, G. N., Zukerberg, L., Nikolic, M., de la Monte, S., Dikkes, P. and Tsai, L. H. (1999). Conversion of p35 to p25 deregulates Cdk5 activity and promotes neurodegeneration. *Nature* **402**, 615-622.

Qu, D., Li, Q., Lim, H. Y., Cheung, N. S., Li, R., Wang, J. H. and Qi, R. Z. (2002). The protein SET binds the neuronal Cdk5 activator p35nck5a and modulates Cdk5/p35nck5a activity. *J. Biol. Chem.* **277**, 7324-7332.

Saito, T., Konno, T., Hosokawa, T., Asada, A., Ishiguro, K. and Hisanaga, S. (2007). p25/cyclin-dependent kinase 5 promotes the progression of cell death in nucleus of endoplasmic reticulum-stressed neurons. *J. Neurochem.* **102**, 133-140.

Sasaki, Y., Cheng, C., Uchida, Y., Nakajima, O., Ohshima, T., Yagi, T., Taniguchi, M., Nakayama, T., Kishida, R., Kudo, Y. et al. (2002). Fyn and Cdk5 mediate semaphorin-3A signaling, which is involved in regulation of dendrite orientation in cerebral cortex. *Neuron* **35**, 907-920.

Sekimoto, T., Fukumoto, M. and Yoneda, Y. (2004). 14-3-3 suppresses the nuclear localization of threonine 157-phosphorylated p27(Kip1). *EMBO J.* **23**, 1934-1942.

Shelton, S. B. and Johnson, G. V. (2004). Cyclin-dependent kinase-5 in neurodegeneration. *J. Neurochem.* **88**, 1313-1326.

Smith, P. D., Mount, M. P., Shree, R., Callaghan, S., Slack, R. S., Anisman, H., Vincent, I., Wang, X., Mao, Z. and Park, D. S. (2006). Calpain-regulated p35/cdk5 plays a central role in dopaminergic neuron death through modulation of the transcription factor myocyte enhancer factor 2. *J. Neurosci.* **26**, 440-447.

Takahashi, S., Saito, T., Hisanaga, S., Pant, H. C. and Kulkarni, A. B. (2003). Tau phosphorylation by cyclin-dependent kinase 5/p39 during brain development reduces its affinity for microtubules. *J. Biol. Chem.* **278**, 10506-10515.

Takano, T., Tsutsumi, K., Saito, T., Asada, A., Tomomura, M., Fukuda, M. and Hisanaga, S. (2010). AATYK1A phosphorylation by Cdk5 regulates the recycling endosome pathway. *Genes Cells* **15**, 783-797.

Tang, D., Yeung, J., Lee, K.-Y., Matsushita, M., Matsui, H., Tomizawa, K., Hatase, O. and Wang, J. H. (1995). An isoform of the neuronal cyclin-dependent kinase 5 (Cdk5) activator. *J. Biol. Chem.* **270**, 26897-26903.

Taniguchi, H. and Manenti, S. (1993). Interaction of myristoylated alanine-rich protein kinase C substrate (MARCKS) with membrane phospholipids. *J. Biol. Chem.* **268**, 9960-9963.

Tian, B., Yang, Q. and Mao, Z. (2009). Phosphorylation of ATM by Cdk5 mediates DNA damage signalling and regulates neuronal death. *Nat. Cell Biol.* **11**, 211-218.

Tomizawa, K., Sunada, S., Lu, Y. F., Oda, Y., Kinuta, M., Ohshima, T., Saito, T., Wei, F. Y., Matsushita, M., Li, S. T. et al. (2003). Cophosphorylation of amphiphysin I and dynamin I by Cdk5 regulates clathrin-mediated endocytosis of synaptic vesicles. *J. Cell Biol.* **163**, 813-824.

Tsutsumi, K., Tomomura, M., Furuichi, T. and Hisanaga, S. (2008). Palmitoylation-dependent endosomal localization of AATYK1A and its interaction with Src. *Genes Cells* **13**, 949-964.

Wei, F. Y., Tomizawa, K., Ohshima, T., Asada, A., Saito, T., Nguyen, C., Bibb, J. A., Ishiguro, K., Kulkarni, A. B., Pant, H. C. et al. (2005). Control of cyclin-dependent kinase 5 (Cdk5) activity by glutamatergic regulation of p35 stability. *J. Neurochem.* **93**, 502-512.

Wen, Y., Yu, W. H., Maloney, B., Bailey, J., Ma, J., Marié, I., Maurin, T., Wang, L., Figueroa, H., Herman, M. et al. (2008). Transcriptional regulation of β-secretase by p25/cdk5 leads to enhanced amyloidogenic processing. *Neuron* **57**, 680-690.

Wu, D. C., Yu, Y. P., Lee, N. T., Yu, A. C., Wang, J. H. and Han, Y. F. (2000). The expression of Cdk5, p35, p39, and Cdk5 kinase activity in developing, adult, and aged rat brains. *Neurochem. Res.* **25**, 923-929.

Xie, Z., Sanada, K., Samuels, B. A., Shih, H. and Tsai, L. H. (2003). Serine 732 phosphorylation of FAK by Cdk5 is important for microtubule organization, nuclear movement, and neuronal migration. *Cell* **114**, 469-482.

Yamada, M., Saito, T., Sato, Y., Kawai, Y., Sekigawa, A., Hamazumi, Y., Asada, A., Wada, M., Doi, H. and Hisanaga, S. (2007). Cdk5-p39 is a labile complex with the similar substrate specificity to Cdk5-p35. *J. Neurochem.* **102**, 1477-1487.

Zhang, J., Cicero, S. A., Wang, L., Romito-Digiacomo, R. R., Yang, Y. and Herrup, K. (2008). Nuclear localization of Cdk5 is a key determinant in the postmitotic state of neurons. *Proc. Natl. Acad. Sci. USA* **105**, 8772-8777.

Zhang, J., Li, H., Yabut, O., Fitzpatrick, H., D'Arcangelo, G. and Herrup, K. (2010). Cdk5 suppresses the neuronal cell cycle by disrupting the E2F1-DP1 complex. *J. Neurosci.* **30**, 5219-5228.

Zheng, M., Leung, C. L. and Liem, R. K. (1998). Region-specific expression of cyclin-dependent kinase 5 (cdk5) and its activators, p35 and p39, in the developing and adult rat central nervous system. *J. Neurobiol.* **35**, 141-159.

doi:10.1093/brain/awr348 Brain 2012: 135; 833–846 | 833

BRAIN
A JOURNAL OF NEUROLOGY

Non-human primate model of amyotrophic lateral sclerosis with cytoplasmic mislocalization of TDP-43

Azusa Uchida,[1] Hiroki Sasaguri,[1] Nobuyuki Kimura,[2] Mio Tajiri,[1] Takuya Ohkubo,[1] Fumiko Ono,[3] Fumika Sakaue,[1] Kazuaki Kanai,[4] Takashi Hirai,[5] Tatsuhiko Sano,[1] Kazumoto Shibuya,[4] Masaki Kobayashi,[1] Mariko Yamamoto,[1] Shigefumi Yokota,[1] Takayuki Kubodera,[1] Masaki Tomori,[5] Kyohei Sakaki,[5] Mitsuhiro Enomoto,[5] Yukihiko Hirai,[6] Jiro Kumagai,[7] Yasuhiro Yasutomi,[2] Hideki Mochizuki,[8] Satoshi Kuwabara,[4] Toshiki Uchihara,[9] Hidehiro Mizusawa[1] and Takanori Yokota[1]

1 Department of Neurology and Neurological Science, Graduate School of Medicine, Tokyo Medical and Dental University, Tokyo 113-8519, Japan
2 Tsukuba Primate Research Centre, National Institute of Biomedical Innovation, Tsukuba 305-0843, Japan
3 Corporation for Production and Research of Laboratory Primates, Tsukuba 305-0843, Japan
4 Department of Neurology, Graduate School of Medicine, Chiba University, Chiba 260-8670, Japan
5 Department of Orthopaedic Surgery, Graduate School of Medicine, Tokyo Medical and Dental University, Tokyo 113-8519, Japan
6 Department of Biochemistry and Molecular Biology, Nippon Medical School, Tokyo 113-8602, Japan
7 Department of Pathology, Graduate School of Medicine, Tokyo Medical and Dental University, Tokyo 113-8519, Japan
8 Department of Neurology, Kitasato University School of Medicine, Kanagawa 228-8555, Japan
9 Laboratory of Structural Neuropathology, Tokyo Metropolitan Institute of Medical Science, Tokyo 156-8506, Japan

Correspondence to: Takanori Yokota,
Department of Neurology and Neurological Science,
Graduate School of Medicine,
Tokyo Medical and Dental University,
Bunkyo-ku, Tokyo 113-8519,
Japan
E-mail: tak-yokota.nuro@tmd.ac.jp

Amyotrophic lateral sclerosis is a fatal neurodegenerative disease characterized by progressive motoneuron loss. Redistribution of transactive response deoxyribonucleic acid-binding protein 43 from the nucleus to the cytoplasm and the presence of cystatin C-positive Bunina bodies are considered pathological hallmarks of amyotrophic lateral sclerosis, but their significance has not been fully elucidated. Since all reported rodent transgenic models using wild-type transactive response deoxyribonucleic acid-binding protein 43 failed to recapitulate these features, we expected a species difference and aimed to make a non-human primate model of amyotrophic lateral sclerosis. We overexpressed wild-type human transactive response deoxyribonucleic acid-binding protein 43 in spinal cords of cynomolgus monkeys and rats by injecting adeno-associated virus vector into the cervical cord, and examined the phenotype using behavioural, electrophysiological, neuropathological and biochemical analyses. These monkeys developed progressive motor weakness and muscle atrophy with fasciculation in distal hand muscles first. They also showed regional cytoplasmic transactive response deoxyribonucleic acid-binding protein 43 mislocalization with loss of nuclear transactive response deoxyribonucleic acid-binding protein 43 staining in the lateral nuclear group of spinal cord innervating distal hand muscles and cystatin C-positive cytoplasmic aggregates, reminiscent of the spinal cord pathology of patients with amyotrophic lateral sclerosis. Transactive response deoxyribonucleic acid-binding protein 43 mislocalization was

Received July 27, 2011. Revised October 26, 2011. Accepted November 14, 2011. Advance Access publication January 17, 2012

an early or presymptomatic event and was later associated with neuron loss. These findings suggest that the transactive response deoxyribonucleic acid-binding protein 43 mislocalization leads to α-motoneuron degeneration. Furthermore, truncation of transactive response deoxyribonucleic acid-binding protein 43 was not a prerequisite for motoneuronal degeneration, and phosphorylation of transactive response deoxyribonucleic acid-binding protein 43 occurred after degeneration had begun. In contrast, similarly prepared rat models expressed transactive response deoxyribonucleic acid-binding protein 43 only in the nucleus of motoneurons. There is thus a species difference in transactive response deoxyribonucleic acid-binding protein 43 pathology, and our monkey model recapitulates amyotrophic lateral sclerosis pathology to a greater extent than rodent models, providing a valuable tool for studying the pathogenesis of sporadic amyotrophic lateral sclerosis.

Keywords: TDP-43; Bunina bodies; cystatin C; cynomolgus monkeys; amyotrophic lateral sclerosis

Abbreviations: AAV = adeno-associated virus; ALS = amyotrophic lateral sclerosis; FTLD = frontotemporal lobar degeneration; HEK = human embryonic kidney; TDP-43 = transactive response DNA-binding protein 43

Introduction

Amyotrophic lateral sclerosis (ALS), also known as Lou Gehrig's disease, is an incurable progressive neurodegenerative disease characterized by muscle weakness and atrophy resulting from the combined loss of upper and lower motoneurons. Most cases of ALS are sporadic, and only 10% of ALS cases are of a familial form. Protein aggregates are one histopathological characteristic of ALS. A breakthrough in understanding ALS pathogenesis was the discovery of the 43-kDa transactive response DNA-binding protein (TDP-43), which was recently identified as the major component of the protein aggregates and of the insoluble fraction in the brains of patients with sporadic ALS and frontotemporal lobar degeneration (FTLD) (Arai *et al.*, 2006; Neumann *et al.*, 2006). TDP-43 is now expected to play an essential role in the pathogenesis of sporadic ALS, possibly equivalent to that of tau and beta amyloid in Alzheimer's disease or α-synuclein in Parkinson's disease.

Human TDP-43 is a highly conserved and ubiquitously expressed 414 amino acid nuclear protein that binds to both DNA and RNA (Ou *et al.*, 1995; Buratti *et al.*, 2001). In normal settings, TDP-43 is a primarily nuclear protein that functions in transcription regulation, alternative splicing and RNA stabilization (Buratti *et al.*, 2008), as well as in microRNA metabolism (Buratti *et al.*, 2010). Pathological TDP-43 can be abnormally truncated, phosphorylated and ubiquitinated, and most TDP-43 is mislocalized from the nucleus to the cytoplasm or neurites (Arai *et al.*, 2006; Neumann *et al.*, 2006). Of note, almost all neurons with cytoplasmic TDP-43 accumulations show a dramatic depletion of normal nuclear TDP-43. Thus, both gain and loss of functions are potential disease mechanisms, either due to the loss of normal nuclear TDP-43 expression, or cytoplasmic mislocalization (Arai *et al.*, 2006; Neumann *et al.*, 2006; Cairns *et al.*, 2007). Therefore, cytoplasmic TDP-43 mislocalization with loss of its nuclear staining is a key feature found in the majority of patients' brains and spinal cords (Arai *et al.*, 2006; Neumann *et al.*, 2006).

TDP-43 strictly regulates its messenger RNA levels by directly binding to an intron in the 3′-untranslated region of its own transcript and enhancing its splicing (Ayala *et al.*, 2010; Polymenidou *et al.*, 2011), however, the expression level of TDP-43 can be upregulated ~1.5-fold (Mishra *et al.*, 2007; Gitcho *et al.*, 2009) in FTLD/ALS. Moreover, mutations in the *TDP-43* gene are associated with familial ALS (Kabashi *et al.*, 2008; Yokoseki *et al.*, 2008), in which TDP-43 is also frequently mislocalized within motoneurons of the spinal cord. These reports support the hypothesis that mislocalization of this protein plays a central role in the disease pathogenesis. The rodent, *Drosophila*, *Ceanorhabditis elegans* and zebrafish models with overexpressed mutant as well as wild-type TDP-43 show severe motor symptoms and wild-type TDP-43 localizes exclusively or primarily to nuclei (Ash *et al.*, 2010; Hanson *et al.*, 2010; Kabashi *et al.*, 2010; Li *et al.*, 2010; Shan *et al.*, 2010; Voigt *et al.*, 2010; Wils *et al.*, 2010; Xu *et al.*, 2010; Swarup *et al.*, 2011), although mutant TDP-43 is more likely to accumulate in the cytoplasm (Swarup *et al.*, 2011). The results of the rodent models suggested that overexpressed nuclear wild-type TDP-43 is toxic, but provide little insight for the significance of mislocalized wild-type TDP-43. Even in mouse models that overexpress wild-type TDP-43 with mutated nuclear localization signals, total human and mouse nuclear TDP-43 was not reduced (Igaz *et al.*, 2011) when compared with that in littermate wild-type controls. Together, these reported mouse models might have a different TDP-43 pathology from that found in patients with ALS. Expecting that a primate model of ALS might more closely reflect the TDP-43 pathology in human patients with ALS, we overexpressed human wild-type TDP-43 in the spinal motoneurons of a non-human primate, the cynomolgus monkey, using an adeno-associated virus (AAV) 1 vector.

Materials and methods

Human subjects

Neurologists clinically diagnosed ALS with the aid of electrophysiological examinations. The clinical diagnosis of definite ALS was based on El Escorial (Brooks *et al.*, 2000) and electrodiagnostic (De Carvalho *et al.*, 2008) criteria and confirmed by neuropathological examination in accordance with published guidelines (Piao *et al.*, 2003).

The patient study protocol was approved by the institutional clinical study committee at Tokyo Medical and Dental University (No. 799). Consent forms for autopsy were obtained from legal representatives of all patients in accordance with the guidelines of the institutional review boards.

Animals

Ten male adult cynomolgus monkeys (*Macaca fascicularis*; 3–7 years old, 3.28–5.10 kg) were bred and treated at Tsukuba Primate Research Centre. The number of monkeys and concentrations of viral stocks were as follows: one monkey was injected with high-dose Flag-TDP-43 AAV1 [1×10^{13} viral genomes (vg)/ml]; six monkeys were injected with low-dose Flag-TDP-43 AAV1 (3×10^{12} vg/ml); three monkeys were injected with low-dose mock AAV1 (3×10^{12} vg/ml) as a negative control. Three monkeys injected with low-dose TDP-43 AAV1 were pathologically examined in the early stage, 3–5 days after the onset of motor symptoms and the other three monkeys were examined in the late stage, 4–7 weeks after injection.

Eleven adult male Fisher rats (10 weeks old, Sankyo-lab) were used. The number of rats and concentrations of viral stocks were as follows: eight rats were injected with low-dose Flag-TDP-43 AAV1 (3×10^{12} vg/ml) and three rats were injected with low-dose control AAV1 (3×10^{12} vg/ml) as a negative control. Three rats injected with TDP-43 AAV1 were pathologically examined in the early stage, 1–2 weeks after injection, and the others were examined in the late stage, 4–9 weeks after injection.

All animal experiments were conducted according to the U.S. National Institutes of Health Guide for the Care and Use of Laboratory Animals, and the Guidelines for the Animal Care and Management of the Tsukuba Primate Research Center and Tokyo Medical and Dental University.

Constructs

Human wild-type TDP-43 was purchased from Invitrogen. The TDP-43 and Flag-TDP-43 fragments were generated by polymerase chain reaction using the following primer pairs: 5′-CCGCTCGAGGCCACCATG GATTAC AAGGATGACGACGATAAGTCTGAATATATTCGGGTAA CCGG-3′ and 5′-CCGCTCGAGCTACATTCCCCAG CCAGAAG ACTTA-3′ for TDP-43, and 5′-CCGCTCGAGGCCACCATGGATTACA AGGATGACGACGAT AAGTCTGAATATATTCGGGTAACCGG-3′ and 5′-CCGCTCGAGCTACATTCCCCAGCCAGAAGACTTA-3′ for Flag-TDP-43, which contained XhoI digestion sites at the 3′- and 5′-ends. The Flag-TDP-43 complementary DNA was subcloned into an expression cassette flanked with AAV2 inverted terminal repeats (Stratagene). The cytomegalovirus (CMV) promoter was used to drive expression.

Adeno-associated virus preparations

Human embryonic kidney (HEK) 293 cells at ~70% confluence were transfected with the AAV1 packaging plasmid pRep2/Cap9 (gift from Dr James M. Wilson, University of Pennsylvania) and adenovirus helper plasmid (Stratagene) at a ratio of 1:1:1. At 6 h after transfection, the culture medium was replaced with fresh medium, and the cells were incubated for 48 h. The cells were then harvested from the culture dishes and pelleted by centrifugation, resuspended in phosphate-buffered saline and subjected to three rounds of freeze–thawing. Cell debris was then pelleted by centrifugation at 1200*g* for 15 min. AAV vectors were purified using ammonium sulphate precipitation and iodixanol (Axis-Shield) continuous gradient centrifugation.

Size-exclusion chromatography was performed using an AKTA Explorer 100 HPLC system (GE Healthcare) equipped with a 2-ml sample loop. A Superdex 200 10/300 GL column (GE Healthcare) was equilibrated with MHA buffer (3.3 mM MES, 3.3 mM HEPES, 3.3 mM NaOAc, 50 mM NaCl, pH 6.5). The vector-containing fractions were loaded onto the column at a flow rate of 0.5 ml/min, and the eluate was collected as 0.5 ml fractions over the duration of one column volume (23 ml). AAV peak fractions were identified by 280/260 nm absorbance and real-time quantitative polymerase chain reaction using vector-specific primers. The purified AAVs were then concentrated further by using Amico Ultra-4 tubes (Ultracel-30k, Millipore) to a final concentration of 1×10^{13} genome copies/ml, as determined by real-time quantitative polymerase chain reaction.

The genome copy number was calculated by TaqMan® PCR (Applied Biosystems). The vectors were treated with Benzonase® and digested with proteinase K (Wako Pure Chemical Industries) for 1 h and purified by phenol–chloroform extraction. The TaqMan® primers and probe were designed as follows: forward primer: 5′-CAGGCTGGT CCAACTCCTA-3′, reverse primer: 5′-GCAGTGGTTCACGCCTGTAA-3′, and probe: 5′-TACCCACCTTGGCCTC-3′. The designed TaqMan® PCR fragment was located in the human growth hormone polyadenylation site in the vector.

Successful viral assembly of control AAV and transgene expression were confirmed by immunoblot analysis using HEK 293 cells infected with AAV (Supplementary Fig. 1), as described below.

HEK-293 cells were cultured in Dulbecco's modified Eagle's medium containing 10% foetal bovine serum with 1% penicillin/streptomycin. The cells in 12-well plates were infected by Flag-TDP-43 AAV1 (5×10^{10} vg/ml). At 48 h after infection, cells were harvested by gentle scraping in lysis buffer [20 mM Tris–HCl, 150 mM NaCl, 1% NP-40, 0.1% deoxicolate, 1% sodium dodecyl sulphate, 1 mM EDTA, 1 mM EGTA, 10 mM β-glycerophosphate, 5 mM NaF and Complete protease inhibitor cocktail (Roche Diagnostics)]. Equal amounts of total cellular protein were mixed with 5× Laemmli sample buffer, denatured at 95°C for 5 min, and separated with 10% sodium dodecyl sulphate polyacrylamide gel electrophoresis. The proteins were transferred to PVDF membranes. After blocking with 3% gelatin (Wako Pure Chemical Industry) in Tris-buffered saline or 5% skimmed milk (Wako Pure Chemical Industry) in Tris-buffered saline-Triton X-100, the membranes were incubated overnight with the following primary antibodies: anti-M2 (1:2000); anti-pan-TDP-43 (1:2000); and anti-VP1, VP2 and VP3 of AAV (1:1000). After incubation with an appropriate horseradish peroxidase-conjugated secondary antibody (Santa Cruz Biotechnology), labelling was detected with the ECL Plus™ Chemiluminescent Detection System (GE Healthcare) or SuperSignal (Thermo Scientific).

Stereotaxic injection of adeno-associated viral vectors

All surgical operations were performed under general anaesthesia. Ketamine hydrochloride (Ketalar, Sankyo) was intramuscularly administered at a dose of 5 mg/kg as a pre-anaesthetic agent, and general anaesthesia was maintained with isoflurane (Forane, Abbott) and oxygen after tracheal intubation. The monkeys were positioned in a stereotaxic frame. After a bilateral laminectomy and opening the dura in the midline at C5–6, AAV vectors were stereotaxically injected into the side ipsilateral to the dominant hand. The injection site was determined and depth of needle insertion was calculated from the preoperatively taken MRI of cervical spinal cord. AAV stock (5 µl) was injected through a 31-gauge needle connected to a 10-µl Hamilton microsyringe in 2 min. The needle remained in place for 10 min and was removed slowly. The dura and skin were sutured and monkeys returned to their individual cages. The monkeys received 0.5 mg/kg butorphanol tartrate (Stadol, Bristol-Myers Squibb) intramuscularly for 3 days to alleviate any postoperative pain.

The rats were anaesthetized with an intraperitoneally administered cocktail of 1.5 ml chloral hydrate (70 mg/ml, Wako Pure Chemical Industry) and 0.1 ml ketamine hydrochloride (70 mg/ml) at a dose of 6 ml/kg. A left side hemi-laminectomy was performed from C4 to C6. On the left side of the C6 segment, 1.5 µl of viral stock was manually injected through sharpened microcapillary glass (PN-30 puller, Narishige) connected via silicone to a 10-µl Hamilton microsyringe at a rate of 0.5 µl/min. The sharpened microcapillary glass remained in place for 3 min and was removed slowly. The skin was sutured, the rats placed on a heating pad until they began to recover from surgery, and then returned to their individual cages.

For detection of the AAV genome in the spinal cord, total DNA was extracted from spinal cord with homogenized buffer containing 0.5% sodium dodecyl sulphate, 10 mM Tris–HCl pH 8.0, and 10 mM EDTA pH 8.0, and polymerase chain reactions were carried out with the following primer pair: 5′-CGCTGTTTTGACCTCCATAGAA-3′ and 5′-AGGCGGTACTTACGTCACTCTTG-3′ for the cytomegalovirus β-globin intron.

Behavioural analysis

For monkeys, to evaluate weakness of the forelimb muscles on the AAV-injected side (the dominant-hand side), we performed the 'apple test'. The front fence of the cage was altered to have two holes and trays on the right and left side. A piece of apple was placed in line from back (monkey side) to front (observer side) on the left or right tray at 3, 6, 9 and 12 cm from the front fence during a session. The monkeys were trained to reach a small piece of apple on the trays through the hole. Four sessions were performed alternately for each side. We analysed how frequently a monkey used his dominant hand to pick up apples before and every week after the operations. We also carefully observed behaviour of the monkeys in daily life every day and recorded video monitoring for 30 min per week.

For rats, to evaluate weakness of the forelimb muscles, we measured grip strength using a special device (Muromachi Kiki) as previously described (Anderson, 2005).

Electrophysiological assessment

The nerve conduction study and needle EMG studies were performed under anaesthesia with a combination of 7 mg/kg ketamine hydrochloride and 1.2 mg/kg xylazine administrated intramuscularly. Nerve conduction studies were performed in the bilateral median nerves using conventional procedures and an EMG Machine (MEB-2300, Nihon-koden). The recording surface electrode was placed over the belly of the thenar eminence with a reference electrode at the metacarpophalangeal joint of the thumb, and compound muscle action potentials were elicited after the stimulation of the median nerve at the wrist. The peak-to-peak amplitudes were measured for all compound muscle action potentials. Nerve conduction studies were examined before AAV injection and every 1 or 2 weeks after. The needle EMG study was performed in the first dorsal interosseous, flexor carpi ulnaris and biceps brachii muscles using a conventional concentric needle electrode used in human studies (TECA Elite, CareFusion), 4–6 weeks after AAV injection.

Neuropathological examinations

Animals were deeply anaesthetized first with intramuscularly administered 7 mg/kg ketamine hydrochloride and then with intravenously administered 25 mg/kg pentobarbital. After confirming the absence of a blink reflex, the spinal cord and skeletal muscles were removed. For neuropathological examination, human and animal spinal cord samples were immersion fixed in 10% neutral buffered formalin, processed conventionally, embedded in paraffin, cut into 4-µm-thick sections and stained with haematoxylin and eosin. For immunostaining, sections were deparaffinized, pretreated in 0.5% periodic acid, autoclaved for 5 min at 121°C and then incubated free-floating overnight at 4°C with the following primary antibodies: M2 (1:500), anti-pan-TDP-43 (1:1000), anti-pS409/410-TDP-43 (1:500), anti-ubiquitin (1:500), anti-p62 (1:500), anti-cystatin-C (1:1000), anti-GFAP (1:500), anti-GLUT-5 (1:500) and SMI31 (1:200). Following brief washes, the sections were sequentially incubated with polymer immunocomplex (Dako)

Immunoreactive elements were visualized by treating sections with 3,3′ diaminobenzidine tetroxide (DAB-4HCl, Dojin Kagaku) with or without nickel ammonium chloride. The sections were then counterstained with haematoxylin. For double-immunostaining, the deparaffinized sections were stained with Sudan Black B to avoid autofluorescence. The free-floating sections were incubated overnight at 4°C in solutions containing the primary antibodies. The sections were then incubated with AlexaFluor 488- or 555-conjugated secondary antibodies (1:500, Invitrogen), and DAPI nuclear stain (1:500, Santa Cruz Biotechnology) for 1 h. All sections were examined using a confocal microscope (NIKON or Carl Zeiss).

Animal anterior root samples were fixed with a mixture of 2.5% glutaraldehyde in 0.1 M phosphate buffer (pH 7.4) at 4°C overnight, and then further fixed in 1% osmium tetroxide in 0.1 M phosphate buffer (pH 7.4) for 1 h. The well-fixed tissues were dehydrated in graded ethanol and embedded in Epon 812 (Poly/Bed® 812, Polyscience). The fixed roots were transversely cut into 1-µm-thick sections and stained with toluidine blue.

For counting of anterior horn neurons in the spinal cord, monkey eighth cervical segments were serially cut at 4-µm thickness, and every fifth section was stained with haematoxylin and eosin. The previous and next serial sections (that is, every fourth and sixth sections) were immunostained with anti-pan-TDP-43 or anti-Flag antibodies. The number and minimum diameters of neurons with nuclei in the lateral or medial nuclear groups in 15 sections were evaluated using the Image J software program from the U.S. National Institutes of Health.

Antibody information

We used the following primary antibodies for immunostaining and immunoblot analyses: mouse monoclonal anti-Flag (M2, Sigma); rabbit polyclonal anti-pan-TDP-43 (10782-1-AP, ProteinTech Group); rabbit polyclonal anti-C-terminal TDP-43 (12892-1-AP, ProteinTech Group); rabbit polyclonal anti-phosphorylated S409/410 TDP-43 (Cosmo Bio); rabbit polyclonal anti-ubiquitin (Dako); rabbit polyclonal anti-cystatin-C (Dako); mouse monoclonal anti-phosphorylated neurofilament (SMI31, Sternberger Monoclonals); rabbit polyclonal anti-glial fibrillary acidic protein (GFAP) (Dako); rabbit polyclonal anti-glucose transporter 5 (GLUT-5, IBL); rabbit polyclonal and mouse monoclonal anti-peripeherin (AB1530 and AB1527, Chemicon); mouse monoclonal anti-neurofilament light (N5139, Sigma) antibody; anti-p62 (GP62-C, Progen); anti-glyceraldehyde-3-phosphate dehydrogenase (GAPDH, Biodesign), and anti-AAV capsid proteins VP1, VP2 and VP3 (Progen Biotechnik).

Sequential biochemical fractionation, dephosphorylation and immunoblot analysis

Frozen frontal cortex or spinal cord (50–250 mg) was homogenized in 10 volumes of buffer A (10 mM Tris–HCl pH 7.5, containing 1 mM

EGTA, 10% sucrose and 0.8 M NaCl). After the addition of Triton X-100 at a final concentration of 1%, the homogenate was incubated for 30 min at 37°C and spun at 100 000*g* for 20 min at 20°C. The pellet was homogenized in 20 volumes of buffer A containing 1% sarkosyl, incubated for 30 min at 37°C and spun at 100 000*g* for 20 min at 20°C. The sarkosyl-insoluble pellet was homogenized in four volumes of buffer A containing 1% CHAPS [3-[(3-cholamidopropyl)dimethylammonio]-1-propanesulphonate] and spun at 100 000*g* for 20 min. The pellet was sonicated in 0.5 volume of 8 mol/l urea buffer, cleared by centrifugation at 100 000*g* for 20 min at 20°C, and used for immunoblotting. The samples before (−) and after (+) treatment with lambda protein phosphatase (1600 U/ml, New England Biolabs) were subjected to 10% sodium dodecyl sulphate polyacrylamide gel electrophoresis. Proteins in the gel were then transferred onto a polyvinylidene difluoride (PVDF) membrane (Millipore). After blocking with 3% gelatin (Wako Pure Chemical Industries) in Tris-buffered saline (50 mM Tris–HCl pH 7.5, 150 mM NaCl), the membranes were incubated overnight with the following primary antibodies: anti-M2 (1:2000); anti-C-TDP-43 (1:1200); anti-phosphorylated S409/410 TDP-43 (1:2000); anti-p62 (1:3000) and anti-GAPDH (1:2000). After incubation with an appropriate horseradish peroxidase-conjugated secondary antibody (Santa Cruz Biotechnology), labelling was detected by a 3,3′diaminobendizene reaction intensified with nickel chloride (Metal-Enhanced DAB Substrate Kit, Thermo Scientific), the ECL Plus™ Chemiluminescent Detection System (GE Healthcare), or SuperSignal (Thermo Scientific).

Quantitative real-time polymerase chain reaction assay

Total RNA was extracted from whole-brain homogenates with Isogen (Nippon Gene). DNase-treated RNA (2.5 μg) was reverse-transcribed with SuperScript® III and random hexamers (Life Technologies). Complementary DNA was amplified by the quantitative TaqMan® system by using the Light Cycler 480 Real-Time PCR Instrument (Roche Diagnostics). The primers and probes specific for Flag-tagged human TDP-43, rat TDP-43 (NM_001011979.2) and monkey TDP-43 (XM_001102660.2) were designed. Relative Flag-human TDP-43 messenger RNA levels were calculated in comparison to endogenous rat or cynomolgus messenger RNA levels. A list of all primers and probes used in this study is provided in Supplementary Table 1.

Statistical analysis

The data obtained from independent experiments are presented as means ± SEM.

Statistical analysis of spinal neuron counts and axonal density among TDP-43-expressed monkey group in early, late stage and control monkey group by one-way ANOVA with Bonferroni's *post hoc* test. $P < 0.05$ was considered significant.

Results

Overexpressing wild-type TDP-43 in the monkey cervical cord leads to progressive motor weakness and muscle atrophy with fasciculation

AAV expressing Flag-tagged TDP-43 (Supplementary Fig. 2) was directly injected into the sixth cervical segment on the dominant-hand side of seven monkeys. All monkeys developed progressive motor weakness and muscle atrophy with marked fasciculation in the forelimb on the injected side (Fig. 1A and B, Supplementary Video 1). Two to 3 weeks after the injection, the TDP-43-expressing monkeys first showed some difficulty in taking time to pick up pieces of apple using the dominant hand on the injected side in the apple test, and changed to use the non-dominant hand (Fig. 1C). On observation by video monitoring, they could reach and grasp the ceiling fence at the onset of clumsiness of picking apples, but 1–3 weeks later could not flex the elbow joint and raise the forelimb, indicating the motor weakness had spread to the proximal muscles (Fig. 1D). In the late stage, 2–5 weeks after the onset, the dominant hand muscles became completely paralysed (Fig. 1A), and muscle weakness and atrophy had spread to the contralateral, un-injected side limb muscles (Fig. 1B and E). One of TDP-43-expressing monkeys showed respiratory failure at the end stage. The control monkeys did not show obvious motor symptoms, indicating surgical procedure or virus toxicity was minimal (Fig. 1C–E and Supplementary Video 2).

Electrophysiological findings

Electrophysiologically, in all TDP-43-expressing monkeys, the compound muscle action potential of the thenar muscle evoked by stimulation of the median nerve at the wrist progressively decreased in size with preservation of conduction velocity, and the muscle became unexcitable in the late stage (Fig. 2A). In contrast, three monkeys injected with control AAV did not show a marked change compound muscle action potential size (Fig. 2A). In TDP-43-expressing monkeys, the compound muscle action potential size on the contralateral side was not changed in the early stage (3–5 days after the onset of motor symptoms), but showed milder reduction of compound muscle action potential size in the late stage (Fig. 2B). Needle EMG revealed robust fasciculation potentials, and denervating potentials of positive sharp waves and fibrillation potentials in the late stage (Fig. 2C).

Cytoplasmic mislocalization with loss of endogenous monkey TDP-43, dystrophic neurites and cystatin C-positive granules in the cytoplasm

Neuropathologically, an anti-Flag antibody widely detected exogenous TDP-43 in neurons from the second cervical to the second thoracic segments on both sides, and was observed in almost all neurons on the injected side from the fourth to eighth cervical segments. Generally, Flag immunoreactivity was not detected in the glial cells. There was no inflammatory reaction except for in the area around the injection site. In the late stage, exogenous TDP-43 was observed in either the nucleus or cytoplasm (Fig. 3A). Pan-TDP-43 staining revealed that most motoneurons with cytoplasmic TDP-43 lost endogenous monkey TDP-43 staining (Fig. 3B), which normally localized in the nucleus (Fig. 3C). Mislocalized TDP-43 was diffusely distributed in the cytoplasm

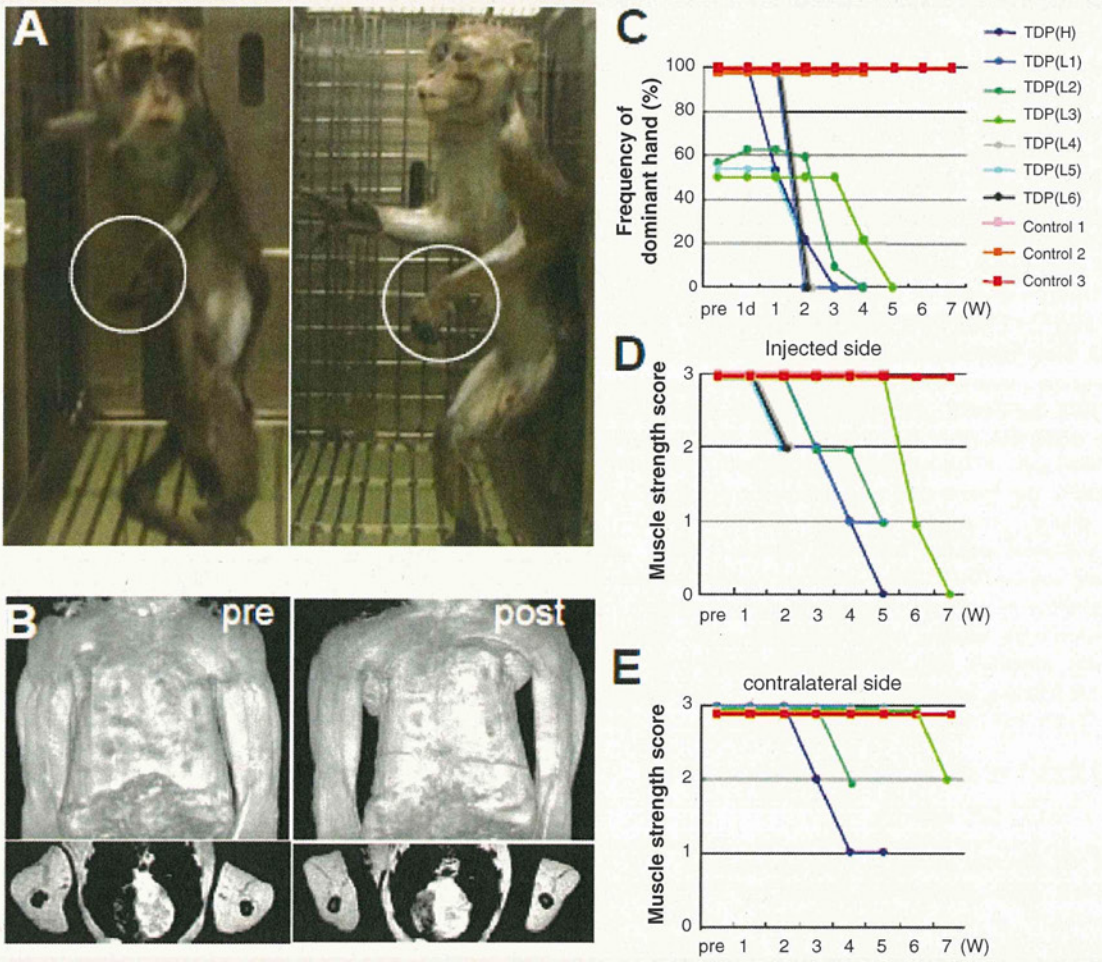

Figure 1 Overexpressing wild-type TDP-43 in the monkey cervical cord leads to progressive motor weakness and muscle atrophy. (**A**) Motor paresis of the forelimb on the injected side (encircled) in TDP-43 AAV-injected monkeys. (**B**) Constructed (*top*) and axial (*bottom*) MRI images of upper arm muscles before (pre) and 4 weeks after (post) injection, indicating a marked muscle atrophy of upper and forearms as well as hand muscles, predominantly on the injected side (left side). (**C**) Apple test. Frequency with which the dominant hand was used to pick up apples. (**D** and **E**) Behavioural analysis assessing muscle strength of forearms on the injected side (**D**) and contralateral side (**E**). A score of 3 indicates that the monkeys can hang on the ceiling fence; score of 2, they can grasp but not hang on the ceiling fence; score of 1, they can raise the forelimb but not reach ceiling fence; score of 0, they cannot raise the forelimb. Measurements that appear to end before the end of the experiment are from the three monkeys that were pathologically examined in the early stage.

and, in some neurons, granularly aggregated (Fig. 3B). Proximal and distal dystrophic neurites were occasionally observed (Fig. 3A and B). Phosphorylation of TDP-43 in the nucleus or cytoplasm was not clear in the early stage, but became obvious in the late stage (Fig. 3D). Anti-ubiquitin and anti-p62 antibodies did not show a clear abnormal signal. Astrogliosis and microgliosis were observed (Supplementary Fig. 3). A small fraction of the motoneurons expressing TDP-43 in the nucleus characteristically displayed coarse cystatin C-positive granules in the cytoplasm (Fig. 3E) in the neurons with exogenously expressed TDP-43 in the nucleus. There were no neurons with co-localized cystatin C-positive granules and TDP-43 aggregates in the cytoplasm. We also observed aberrant accumulation of phosphorylated neurofilaments (Fig. 3F) and peripherin (Supplementary Fig. 4) in the cytoplasm of spinal motoneurons, a common pathological feature in patients with ALS (Munoz *et al.*, 1988; Corbo and Hays, 1992). Immunostaining with an anti-Flag antibody identified its nuclear or cytoplasmic immunoreactivity in some Betz cells in the precentral gyrus restricted to the forelimb area contralateral to the injection. This Flag immunoreactivity was not observed in other cortical areas (including hippocampus and frontal lobe, which are preferentially affected in patients with FTLD), thalamus, basal ganglia and white matter, or in glial cells (Supplementary Fig. 5).

Characteristic regional mislocalization of TDP-43 in motoneurons of the anterior horn similar to amyotrophic lateral sclerosis spinal cords

In the early stage, 3–5 days after the onset of hand clumsiness, TDP-43 mislocalization of diffuse staining pattern was observed in

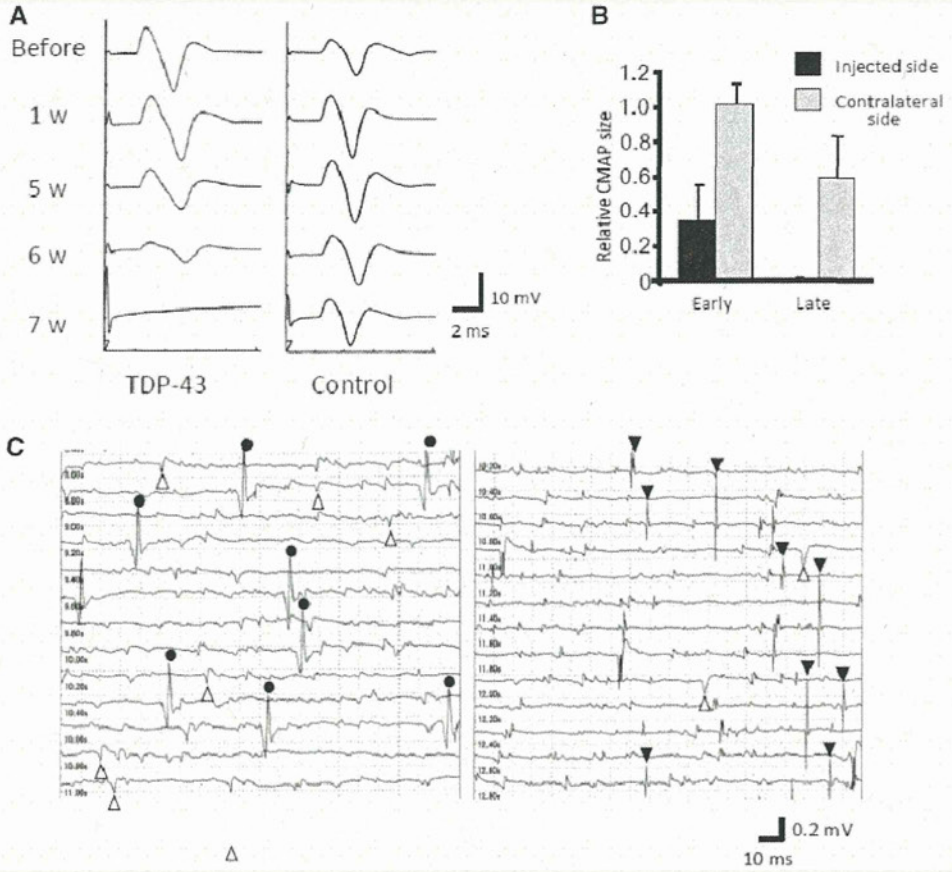

Figure 2 Electrophysiological findings for motor symptoms of the monkeys. (**A**) Compound muscle action potentials (CMAPs) in the thenar muscle after stimulation of the median nerve at the wrist. They gradually decreased in size, and became inexcitable in the late stage. There was no change of compound muscle action potential size in the control monkey. (**B**) Ratio of the compound muscle action potential size 3–5 days after the onset (early stage) or 2–5 weeks after the onset (late stage) to the size before injection. In the early stage, there was no reduction in compound muscle action potential size on the contralateral side, but moderately attenuated in the late stage. (**C**) Needle EMG findings of the forearm muscle. Circles indicate fasciculation potentials; open triangles, positive sharp waves; filled triangles, fibrillation potentials.

most motoneurons in the lateral nuclear group of the anterior horn. In contrast, almost all neurons in other areas of the spinal cord including the posterior horn showed flag signal of exogenously expressed TDP-43 only in the nucleus (Fig. 4A and D). Importantly, the contralateral lateral nuclear group also exhibited TDP-43 mislocalization on the side of forelimb that did not yet show obvious motor symptoms (Supplementary Fig. 6). Signals of exogenous Flag-TDP-43 were detected by real-time polymerase chain reaction on the contralateral half of the spinal cord (Supplementary Fig. 7). However, this distribution indicates that this regional selectivity is not due to differences in the concentration of the injected AAV, but rather is due to properties of the affected neurons. In the late stage, 2–5 weeks after onset, the percentage of motoneurons with TDP-43 mislocalization decreased ~47% in the lateral nuclear group, and was <2% in the ventromedial nuclear group (Figs 3B and 4D). The number of large motoneurons ($\geqslant 20\,\mu m$) in the early stage in this lateral nuclear group did not change, but in the late stage, was reduced by ~42% (Fig. 4B, C and E). In contrast, the reduction in the number of large neurons in the ventromedial nuclear group was not significant (control, 1.78 ± 0.20 versus TDP-43, 1.68 ± 0.18/section, $P = 0.80$). Astrogliosis was also more prominent in the lateral area than in the ventromedial area of the anterior horn (data not shown). Motoneuronal degeneration of the lateral nuclear group was also confirmed by studying the anterior roots of the eighth cervical segment, which showed frequent myelin ovoids and loss of large myelinated axons ($\geqslant 8\,\mu m$) in the late stage, although they were almost normal in the early stage (Fig. 5A–C). This axonal loss in the anterior roots is consistent with pathological change of the thenar muscle, showing numerous small angulated atrophic fibres (Fig. 5D).

We furthermore examined whether such a regional change of TDP-43 mislocalization occurs in spinal cord of nine patients with ALS with upper limb weakness and hand muscle atrophy. TDP-43 mislocalization was observed much more in the lateral nuclear group than in the ventromedial nuclear group of the cord at the eighth cervical segment (Fig. 6A–C).

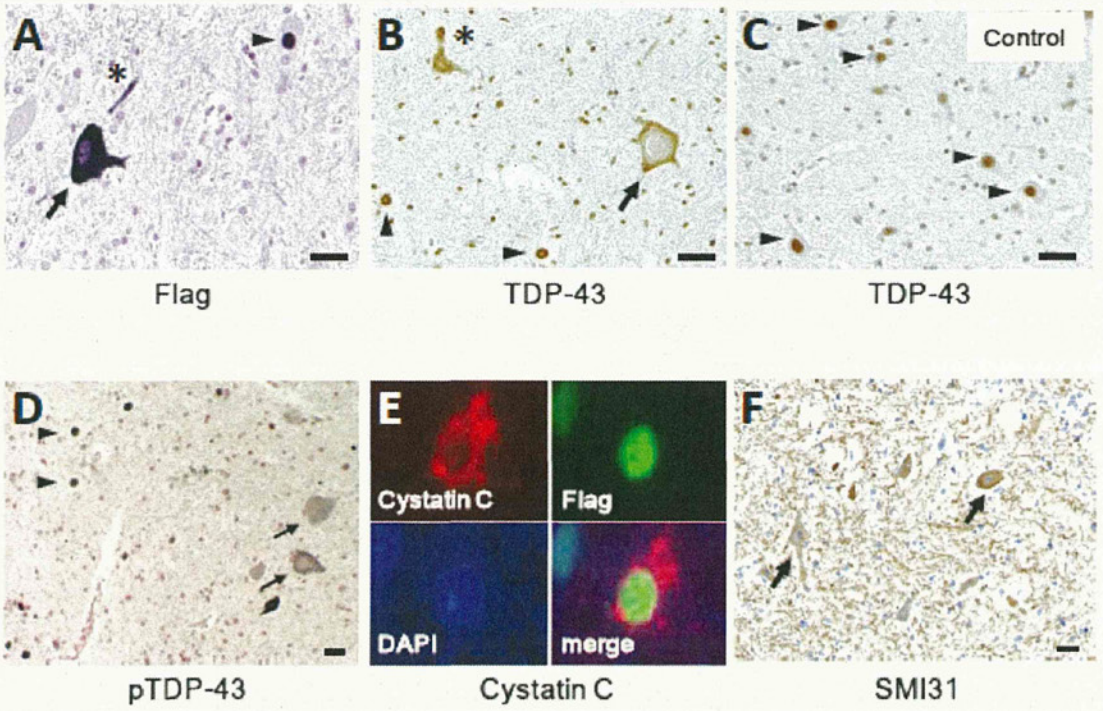

Figure 3 Neuropathological findings of monkey spinal cords of TDP-43–overexpressed monkeys at the late stage (**A**, **D–F**), and control with mock AAV (**C**). (**A–D**) TDP-43-overexpressed spinal cord immunostaining using antibodies to Flag (**A**), pan-TDP-43 (**B**) and pS409/410 TDP-43 (**D**) demonstrated mislocalization in cytoplasm (arrows), and dystrophic neurites (asterisks) as well as normal localization in nuclei (arrowheads), whereas normal spinal cord showed only nuclear localization of TDP-43. (**E**) Co-labelling of a motoneuron expressing TDP-43 in the nucleus with antibodies to cystatin C (red) and Flag (green). The nucleus is labelled with DAPI. (**F**) Immunostaining using SMI31 revealed the aberrant presence of phosphorylated neurofilament in the neuronal cytoplasm (arrows). Scale bars: 20 μm. Immunostainings of spinal cord with control mock AAV using the antibodies to Flag, pS409/410 TDP-43, cystatin C and SMI31 are shown in Supplementary Fig. 7.

Interspecies differences in TDP-43 pathology in rodents and primates

To investigate interspecies differences in TDP-43 pathology, we injected the identical TDP-43-expressing AAV at the same concentration into rat cervical cords. Expression level of Flag-TDP-43 messenger RNA around the injection site in rat spinal cord was >20-fold higher than that of endogenous TDP-43 level, and this fold change was similar to that in monkey spinal cord (Fig. 7A). Rats injected with TDP-43 AAV showed progressive motor weakness (Fig. 7B), measured by grip strength. Importantly, exogenous TDP-43 was observed only in the nuclei of motoneurons in both early (14 days after injection of AAV) and late (4 weeks after injection of AAV) stages (Fig. 7C). Since mislocalization of TDP-43 in the monkey spinal cords was more prominent in the early stage (14 days), we also examined the pathology of rat spinal cords at a very early stage (7 days); however, the weak Flag immunoreactivity was still limited to the nucleus of motoneurons (data not shown). Furthermore, this rat model failed to exhibit cystatin C-positive aggregates, dystrophic neurites, or aberrant accumulation of phosphorylated neurofilaments in the cytoplasm of spinal motoneurons (Fig. 7D). These neuropathological findings indicate that this rat model was less similar to human ALS than our monkey model in TDP-43 localization and other characteristic features of ALS.

Detection of the 25-kDa C-terminal fragment and phosphorylated TDP-43 in the early stage

Biochemically, immunoblot analysis of monkey spinal cord demonstrated that the exogenous Flag-tagged TDP-43 became much more insoluble than endogenous TDP-43 (Fig. 8A). The phosphorylation of TDP-43 was unclear in the early stage (Fig. 8B) but clearly detected later (Fig. 8C). Neither a C-terminal nor a phosphospecific TDP-43 antibody detected the 25-kDa C-terminal fragment (Fig. 8A–C). These suggest that neither phosphorylation of TDP-43 or its 25-kDa C-terminal fragment in spinal cord is necessary to initiate motoneuronal dysfunction and degeneration in our monkeys.

Discussion

Frequent mislocalization of TDP-43 in the cytoplasm and loss of its nuclear staining are major pathological hallmarks in the histological